Available online at www.sciencedirect.com
ScienceDirect
Journal of Power Sources 180 (2008) 553–560
JOURNAL OF POWER SOURCES
www.elsevier.com/locate/jpowsour

Synthesis and characterization of Carbon Nano Fiber/$LiFePO_4$ composites for Li-ion batteries

M.S. Bhuvaneswari [a,*], N.N. Bramnik [a], D. Ensling [a], H. Ehrenberg [a,b], W. Jaegermann [a]

[a] *Darmstadt University of Technology, Institute of Materials Science, Petersenstrasse 23, 64287 Darmstadt, Germany*
[b] *IFW Dresden, Institute for Complex Materials, Helmholtzstr, 20, 01069 Dresden, Germany*

Received 22 September 2007; received in revised form 17 January 2008; accepted 26 January 2008
Available online 16 February 2008

Abstract

Carbon Nano Fibers (CNFs) coated with $LiFePO_4$ particles have been prepared by a non-aqueous sol–gel technique. The functionalization of the CNFs by HNO_3 acid treatment has been confirmed by Raman and XPS analyses. The samples pure $LiFePO_4$ and $LiFePO_4$–CNF have been characterized by XRD, SEM, RAMAN, XPS and electrochemical analysis. The $LiFePO_4$–CNF sample shows better electrochemical performance compared to as-prepared $LiFePO_4$. $LiFePO_4$–CNF (10 wt.%) delivers a higher specific capacity (~140 mAh g^{-1}) than $LiFePO_4$ with carbon black (25 wt.%) added after synthesis (~120 mAh g^{-1}) at 0.1C.

Keywords: Carbon Nano Fiber; $LiFePO_4$; Raman analysis; X-ray photo electron spectroscopy; Electrochemical analysis

1. Introduction

The commercially used cathode material $LiCoO_2$ in lithium-ion batteries is associated with problems such as high cost, toxicity, and safety risks in large scale applications which created a paramount need for an alternative cathode candidate [1]. Recently lithium 3d-metal orthophosphates have gained a substantial interest as positive cathode materials [2–5]. Among the orthophosphates $LiFePO_4$ exhibits several properties such as environmental friendliness, low price, non-toxicity, and exceptional stability, which perfectly matches with the needs to replace $LiCoO_2$ [6,7]. However, a major limitation of this material is its poor rate performance, because of its low electronic conductivity [8–11]. Current research on $LiFePO_4$-based materials aims towards improving the rate performance by reducing its particle size and by effective carbon coating [8–11]. Various synthesis methods such as sol–gel, co-precipitation, carbothermal reduction, etc. have been utilized to optimize the particle size of $LiFePO_4$, and positive results have been reported [8–13]. Different organic additives for carbon coating around $LiFePO_4$ particles and cation doping into the olivine structure have also been tried to enhance the intrinsic electronic conductivity of $LiFePO_4$ [14,15]. Hu et al. reported that the structure of the residual carbon on the $LiFePO_4$ particles is important for the electrochemical performance [14]. Zaghib et al. reported that a critical factor towards improving the performance is the carbon content in the electrode, which is related to electrical conductivity and networking between particles [16]. A new approach to enhance the effects of carbon content and coating of $LiFePO_4$ particles is reported here, based on the addition of functionalized Carbon Nano Fibers (CNFs) during the sol–gel synthesis of $LiFePO_4$. It has been reported in literature [17] that carbon is found efficient to reduce the resistivity of $LiFePO_4$ if sp^3 bonding in carbon is very small hence in the present study Carbon Nano Fiber has been used instead of amorphous carbon. It has been found that the functionalized CNFs can be coated with $LiFePO_4$. For comparison, pure $LiFePO_4$ has also been prepared by a non-aqueous sol–gel method. $LiFePO_4$-coated CNF electrodes without additional carbon black show excellent electrochemical performance and are compared to electrodes, prepared from pure $LiFePO_4$ with additional carbon black. The samples have been characterized

* Corresponding author. Tel.: +49 61 51 16 63 53; fax: +49 61 51 16 63 08.
E-mail address: bhuvana.siva@gmail.com (M.S. Bhuvaneswari).

0378-7753/$ – see front matter © 2008 Elsevier B.V. All rights reserved.
doi:10.1016/j.jpowsour.2008.01.090

by thermogravimetric–differential thermal analysis (TG–DTA), XRD, SEM, Raman spectroscopy, XPS and electrochemical analyses.

2. Experimental

$LiFePO_4$ has been prepared from a mixture of $Li(CH_3COO)\cdot 2H_2O$ (lithium acetate), $Fe(CH_3COO)_2$ (iron acetate), H_3PO_4 (phosphoric acid) and ethylene glycol. The synthesis conditions reported by Yang et al. with slight modifications have been adopted [13]. The precursors were dissolved in ethylene glycol at a molar ratio of 1:1:1. After rigorous stirring the resulting gel has been heat treated at 700 °C with a heating rate of 10 °C min^{-1} in argon atmosphere for 12 h (here after to be named as pure $LiFePO_4$).

The functionalization of pyrolytically stripped Carbon Nano Fibers (commercial grade from Electrovac AG, Austria, with a diameter and length of 100–200 nm and >20 μm, respectively) was achieved by treating the Carbon Nano Fiber with conc. HNO_3 at 70 °C for 24 h. After treatment the suspension of C-Fibers in HNO_3 was diluted with deionized water, filtered, washed with water and dried at 110 °C in open air atmosphere (here after the acid treated Carbon Nano Fiber to be named simply as CNF).

10 wt.% of CNF has been added with the same precursors used for preparing pure $LiFePO_4$ during sol–gel preparation, and the sol–gel has been stirred for one week in order to get better contact of $LiFePO_4$ particles with CNF. The gel has been heat treated at 600 °C with a heating rate of 10 °C min^{-1} in argon atmosphere for 12 h (here after will be named as $LiFePO_4$–CNF).

TG–DTA measurements have been performed (TGA92-Setaram) from 0 to 1000 °C at a heating rate of 10 °C min^{-1} under argon atmosphere. The samples were tested by X-ray powder diffraction using a STOE STADI/P powder diffractometer (Mo $K\alpha_1$ radiation). A scanning electron microscope Philips XL 30 FEG has been used to observe the particles morphology. To determine the carbon content elemental analysis has been performed using VarioEL III CHN elemental analyzer. Raman measurements have been carried out by Labram 800 HR open microscope from Horiba Jobin Yvon with a laser wavelength of 488 nm. The XPS studies have been performed using an Escalab 250 Spectrometer with a monochromatized Al anode. Electrochemical studies were carried out with a multichannel potentiostatic–galvanostatic system VMP (PerkinElmer Instruments, USA). Swagelok-type cells were assembled in an argon-filled dry box with water and oxygen contents less than 1 ppm. A pure $LiFePO_4$ cathode composite has been fabricated as follows: 60% active material, 25% acetylene carbon black and 15% PTFE as binder were intimately mixed, ground in an agate mortar and pressed onto an Al-mesh (resulting electrodes contain about 3 mg of active compound). The $LiFePO_4$–CNF cathode consists of 90% $LiFePO_4$ (10 wt.% CNF) and 10% PTFE. 2.31 wt.% and 12.29 wt.% carbon (calculated from elemental analysis) contents for the pure $LiFePO_4$ and the $LiFePO_4$–CNF samples, respectively, have been included for the cathode active mass calculation, lithium metal was used as anode and the electrolyte was 1 M $LiPF_6$ in 2:1EC/DMC.

3. Results and discussion

3.1. Functionalization of CNFs

Carbon Nano Fibers have been functionalized by concentrated HNO_3 before they were added to the gel, to get better adhesion to the $LiFePO_4$ particles by introducing compatible functional groups on the Carbon Nano Fiber surface [18]. This treatment with acid leads to a partial oxidation of the surface and the formation of oxidized groups like C–OH– or C=O. The functionalization has been confirmed by Raman and XPS analyses.

3.1.1. Raman analysis

The Raman spectra of pristine CNF and HNO_3 treated CNF are shown in Fig. 1. The band in the region of 2500–2900 cm^{-1} is the second order D-band (D^*-band), which depends on the 3-dimensional packing scheme. The group of peaks observed in the range of 1550–1660 cm^{-1} is called the graphite band (G-band), which is most pronounced for a high degree of symmetry and ordered structure in a carbon material. The bands observed from 1250 to 1450 cm^{-1} corresponds to a disorder-induced phonon mode (D-band) with a high intensity for disordered carbon materials. The relative intensities I_D/I_G and I_{D^*}/I_G can be used qualitatively to characterize the order of carbon materials and are also a measure for the amount of carbon defects in the nanofibers due to the presence of functional groups [19,20]. Higher ratios of I_D/I_G or I_{D^*}/I_G correspond to a lower degree of order in the CNFs [19]. The characteristic Raman bands observed for pristine and HNO_3 treated CNF are tabulated in Table 1. The I_D/I_G ratio for HNO_3 treated CNFs is high compared to the pristine CNFs which confirms the functionalization of the Carbon Nano Fibers, an important factor for networking $LiFePO_4$ particles with the surface of Carbon Nano Fibers.

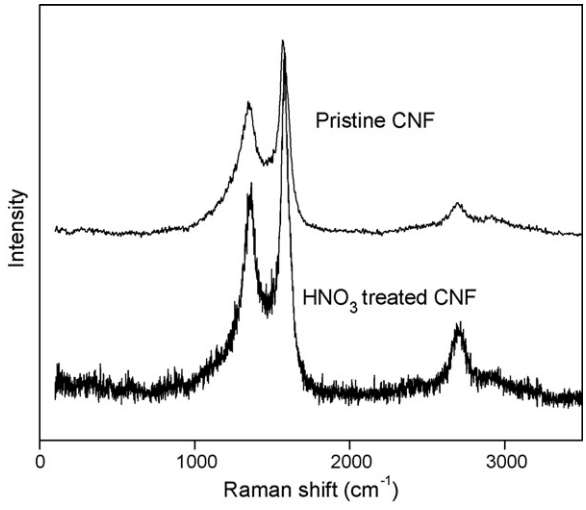

Fig. 1. Raman spectra for pristine and functionalized CNFs.

Table 1
Raman wave numbers and corresponding band assignments for pristine and functionalized CNFs

Sample	D line (cm^{-1})	G peak (cm^{-1})	D^* peak (cm^{-1})	D/G value (cm^{-1})	D^*/G value (cm^{-1})
Pristine CNF	1349.2	1570.3	2698.9	0.394	0.116
Functionalized CNF	1358.1	1575.0	2703.9	0.490	0.179
$LiFePO_4$–CNF	1336.4	1578.8	2651.9	0.400	0.146

3.1.2. XPS analysis

The XPS survey spectra of pristine CNF and functionalized CNF (not shown) indicates that carbon and oxygen are the dominant species comprising the carbon fiber surfaces. The corresponding high resolution carbon C1s and oxygen O1s XPS spectra are shown in Fig. 2a and b, respectively. The C1s spectrum of pristine CNFs shows the graphitic carbon peak at 284.6 eV. The C1s spectrum of pristine CNF is asymmetric in nature and the O1s peak has been deconvoluted into two main peaks, corresponding to C=O groups (∼531.1 eV) and C–OH groups (∼532.7 eV) [21]. This indicates that the pristine CNFs have already been oxidized to an appreciable extent, a normal behavior of Carbon Nano Fibers [21]. The HNO_3 treated CNFs indicate a significant change in the XPS spectra of carbon C1s and oxygen O1s compared to pristine CNFs. Considering the C1s profile, the main emission (284.6 eV) broadens towards higher binding energy (B.E.) and there is clearly enhanced emission of a feature near 288 eV. The former observation is consistent with an increased presence of hydroxyl groups, whereas the latter trend is consistent with an increase in the relative amount of carboxyl functional groups [21]. The O1s spectra become more asymmetric and broader towards lower binding energy, consistent with an increase in the relative proportion of C=O and C–OH groups [21]. The O/C atomic ratio of pristine CNFs and HNO_3 treated CNFs are ∼0.02 and ∼0.234, respectively. The increase in the O/C atomic ratio confirms the functionalization of Carbon Nano Fibers by HNO_3 acid treatment [22].

3.2. Synthesis and characterization of pure $LiFePO_4$ and $LiFePO_4$–CNF

3.2.1. TG–DTA analysis

Fig. 3 shows the thermogravimetric–differential thermal analysis curves for the sol–gel precursors of pure $LiFePO_4$. The TG curves indicate one sharp mass-loss peak between 129 and 245 °C ($\Delta m/m = 83.18$ wt.%). This mass-loss process is related to exothermic and endothermic peaks in the DTA curve. The exothermic peaks at 96.6, 218.6, 330.4 and 422.3 °C are due to the thermal decomposition of ethylene glycol and acetate precursors. The endothermic peaks observed at 325.9 and 368.5 °C correspond to the elemental carbon formation [23–25]. An endothermic peak has been observed at 422.3 °C for pure $LiFePO_4$, but no appreciable weight loss is observed in the TG curve above 245 °C, suggesting that the crystallization of $LiFePO_4$ takes place at this temperature. A single phase with an ordered olivine structure will be realized even at 550 °C, but the effective amorphous carbon coating from the precursors (without the addition of CNF) will be obtained when the samples were heat treated at 700 °C, hence the synthesis temperature for pure $LiFePO_4$ has been chosen as 700 °C [4,13]. The synthesis tem-

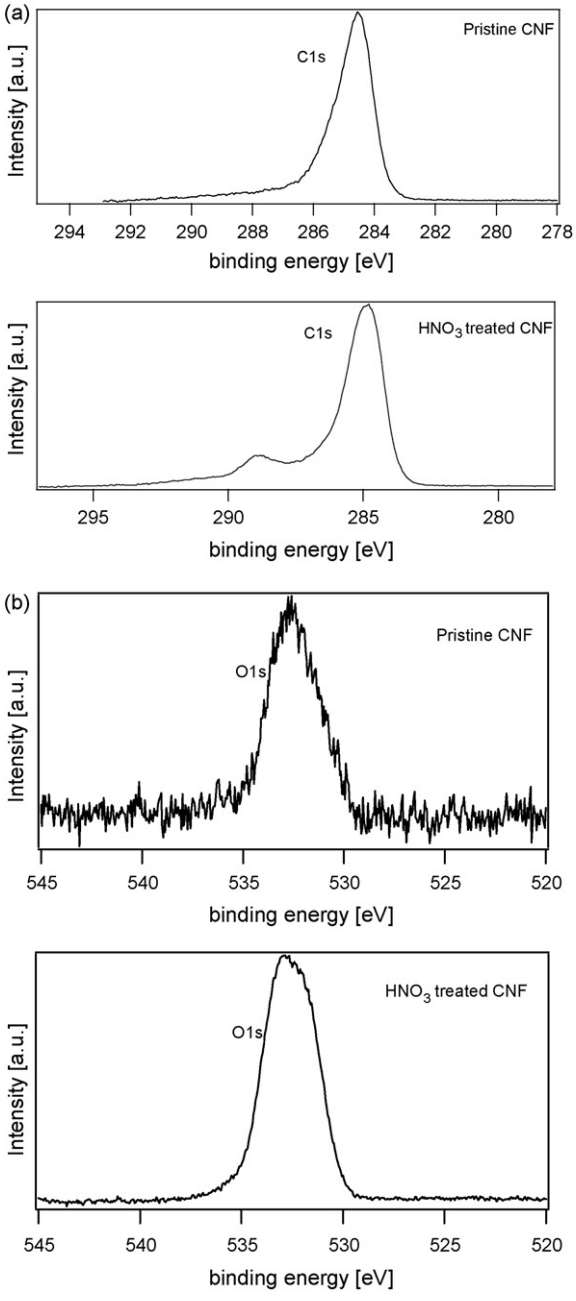

Fig. 2. XPS spectra (a) in the region of C1s for pristine and HNO_3 treated CNF; (b) in the region of O1s for pristine and HNO_3 treated CNF.

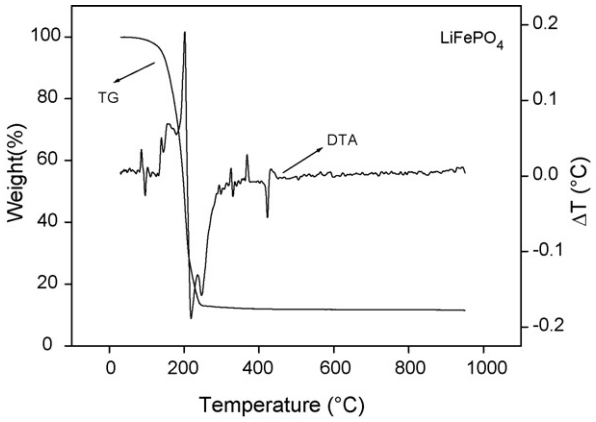

Fig. 3. TG/DTA curves of $LiFePO_4$ obtained under argon atmosphere at a heating rate of 10 °C min^{-1}.

perature for $LiFePO_4$–CNF has been chosen as 600 °C as we are not interested in amorphous carbon coating for $LiFePO_4$–CNF samples.

3.2.2. XRD analysis

The XRD patterns for pure $LiFePO_4$ (Fig. 4a) and $LiFePO_4$–CNF (Fig. 4b) indicate the good crystalinity of samples. All reflections can be indexed based on the orthorhombic $LiFePO_4$ crystallizing in the space group *Pnma*. A slight contribution from the amorphous part can be identified in the diffraction pattern of $LiFePO_4$–CNF composite, which can be attributed to the presence of amorphous C-Fibers in the sample. The olivine-like structure was confirmed by Rietveld analysis performed with the structural model taken from Ref. [26]. The unit cell parameters obtained for $LiFePO_4$ ($a = 10.3281(3)$ Å, $b = 6.0080(2)$ Å, $c = 4.6947(1)$ Å) and for $LiFePO_4$–CNF ($a = 10.3314(7)$ Å, $b = 6.0064(4)$ Å, $c = 4.6996(4)$ Å) are in a good agreement with the ones reported in literature [26].

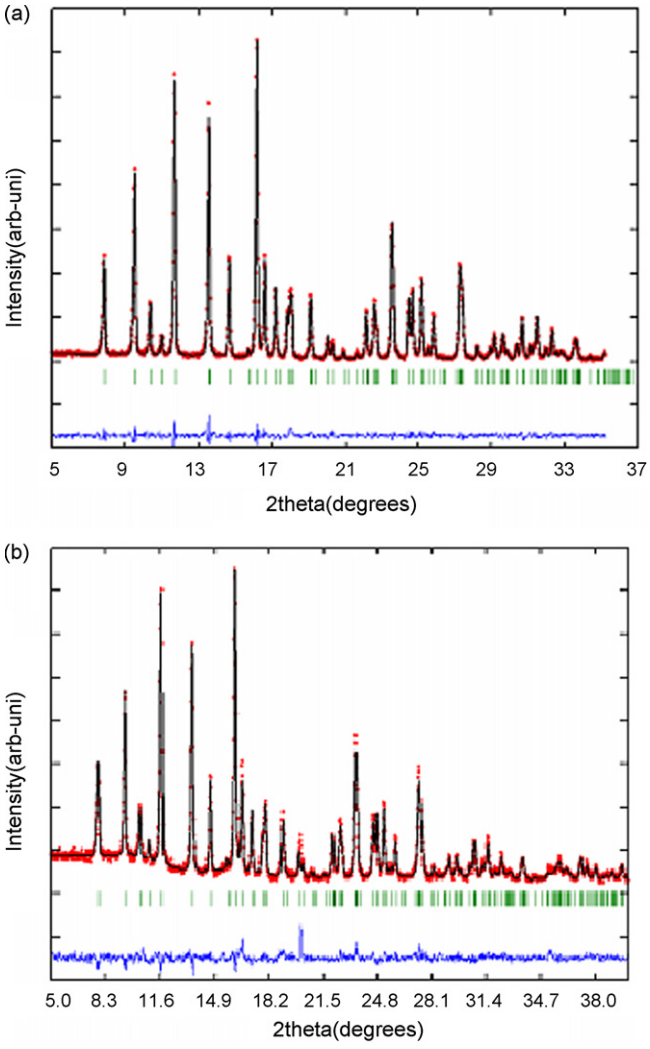

Fig. 4. Rietveld refinement of (a) $LiFePO_4$ and (b) $LiFePO_4$–CNF samples prepared by a non-aqueous sol–gel method.

3.2.3. SEM

The scanning electron micrographs of pure $LiFePO_4$ are shown in Fig. 5a and b. The SEM pictures indicate the agglomeration of particles and grain dimensions of about 500 nm to 1 μm. The SEM pictures of $LiFePO_4$–CNF are shown in Fig. 6a and b, which indicate a non-homogeneous coating of $LiFePO_4$ particles smaller than 200 nm over Carbon Nano Fibers. The reduction in particle size in comparison with pure

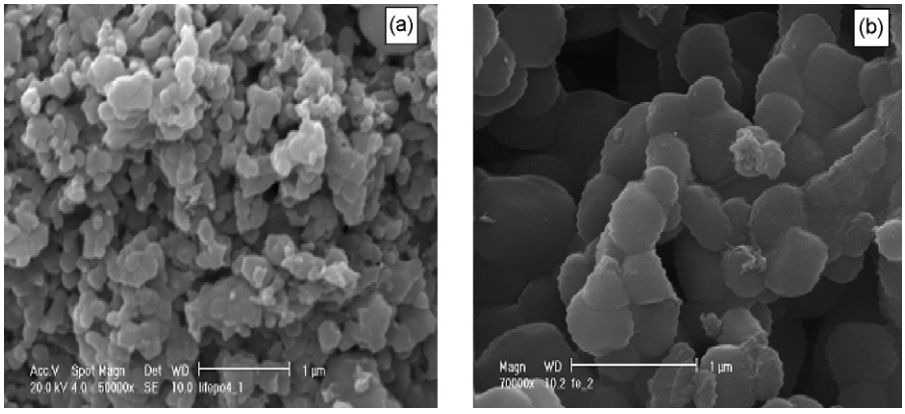

Fig. 5. (a and b) SEM images of CNF free $LiFePO_4$.

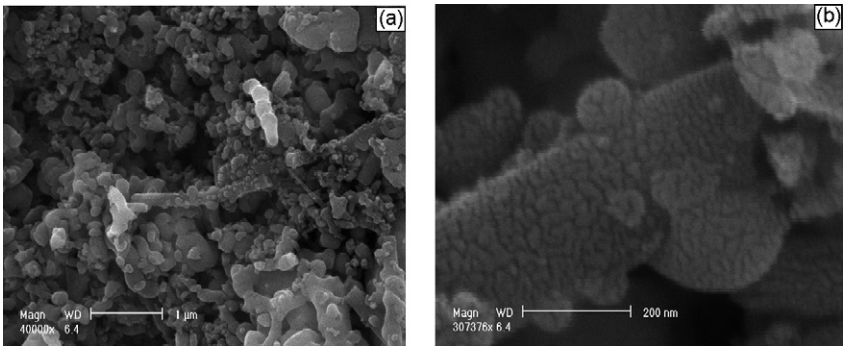

Fig. 6. (a and b) SEM images of CNF added $LiFePO_4$.

$LiFePO_4$ is mainly due to the lower synthesis temperature for $LiFePO_4$–CNF.

3.2.4. Raman analysis

The Raman spectra of $LiFePO_4$ and $LiFePO_4$–CNF are shown in Fig. 7. The carbon lines at 1339.3 and at 1579.7 cm^{-1} are significantly screened by the characteristic Raman lines for both the pure $LiFePO_4$ and the $LiFePO_4$–CNF samples. The weak carbon lines, which appear for "pure" $LiFePO_4$ are due to the presence of residual carbon from the organic precursors. The intramolecular stretching modes of PO_4^{3-} are recorded at 581, 987.5 and 1051 cm^{-1}. Only a slight difference in the characteristic Raman wave numbers (shifted by 4–6 cm^{-1}) of $LiFePO_4$ has been observed between pure $LiFePO_4$ and $LiFePO_4$–CNF samples due to interactions with the CNFs. $LiFePO_4$–CNF shows a second order D-band (D^*). The intensity ratios D/G and D^*/G have been calculated and are also tabulated in Table 1. The D/G and D^*/G values of $LiFePO_4$ with 10 wt.% CNF are higher when compared to pristine CNFs but lower than for the HNO_3 treated CNFs. An intermediate value for $LiFePO_4$–CNF is expected, because in addition to the 10 wt.% CNFs amorphous carbon is also present from the organic precursors. These intensity ratios are not reliable to evaluate the sp^3 and sp^2 content in samples with amorphous carbon in it [17].

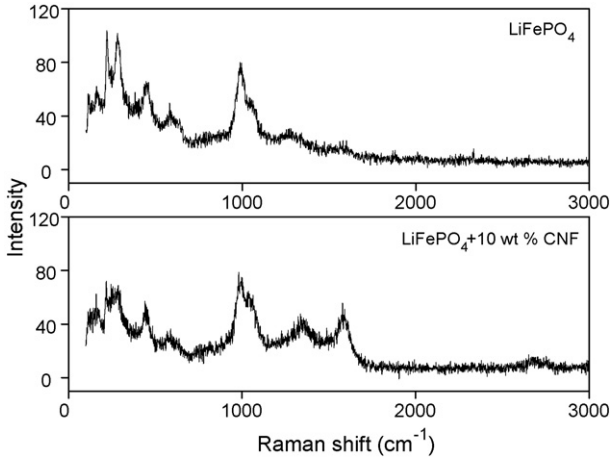

Fig. 7. Raman spectra of pure $LiFePO_4$ and $LiFePO_4$–CNF samples.

3.2.5. XPS analysis

The XPS spectra of pure $LiFePO_4$ and $LiFePO_4$–CNF samples in the binding energy range of O1s, C1s and P2p are shown in Figs. 8 and 9 respectively. Their corresponding binding energies are tabulated in Table 2. The $LiFePO_4$–CNF sample shows the appearance of a shoulder at higher binding energies of O1s spectra which is absent for the pure sample. We therefore assign this emission to the oxidation modified CNT containing C=O and C–OH surface moieties [22]. The main emission represents the $LiFePO_4$ oxide ions in $LiFePO_4$. The carbon C1s line is deconvoluted into three contributions for both the CNF free

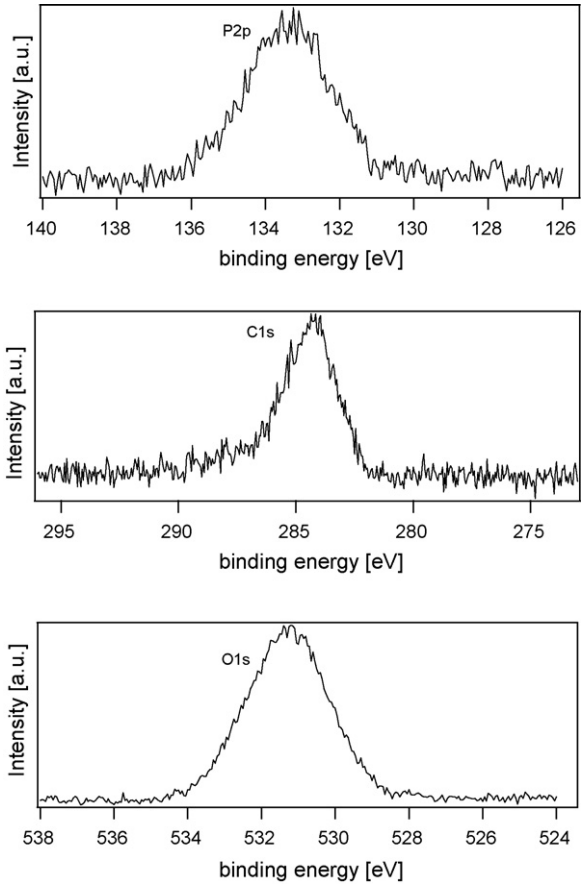

Fig. 8. XPS spectrum in the region of P2p, C1s, O1s for pure $LiFePO_4$.

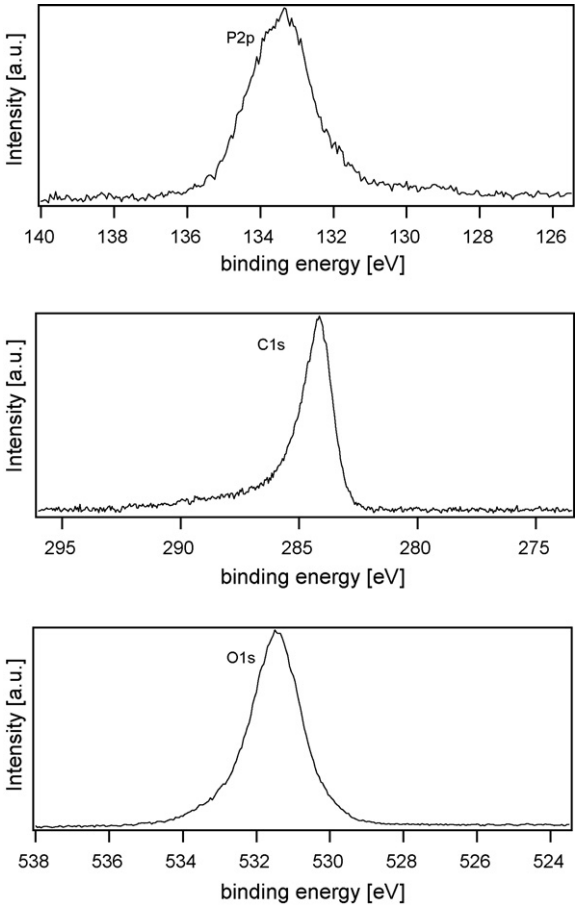

Fig. 9. XPS spectrum in the region of P2p, C1s, O1s for $LiFePO_4$–CNF.

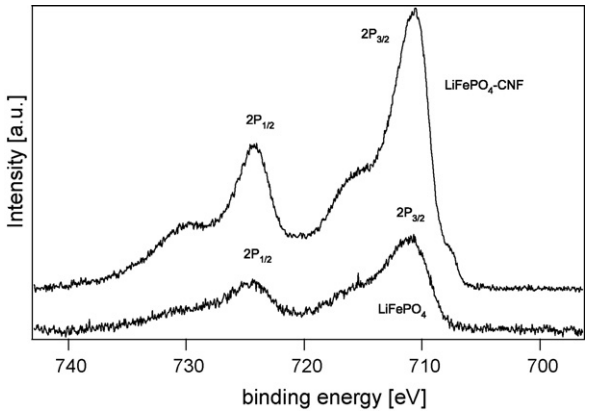

Fig. 10. XPS spectrum in the region of Fe2p for pure $LiFePO_4$ and $LiFePO_4$–CNF.

and CNF added samples. The graphitic carbon emission for $LiFePO_4$–CNF sample is observed at 284.7 eV. The asymmetric behavior of the C1s line for pure $LiFePO_4$ is due to the presence of amorphous carbon, as observed in Raman analysis. The P2p emission corresponds to the PO_4^{3-} group and the Fe/P ratio (1.06) is consistent with the compound stoichiometry for both pure $LiFePO_4$ and $LiFePO_4$–CNF samples [27].

The XPS spectra in the region of Fe2p for pure $LiFePO_4$ and $LiFePO_4$–CNF samples are shown in Fig. 10. The binding energy scale is presented as measured. A single low intensity peak on the low binding energy side of the envelope is due to the formation of Fe ions with a lower than normal oxidation state by the production of defects in neighboring sites [28]. For transition metal ions with partially filled d-states the appearance of satellite peaks (mentioned as shoulder peaks in literature) is a characteristic feature, and for our samples we observe this satellite peaks along with the main Fe2p peaks at higher binding energies of Fe2p (Table 2). The Fe2p emission is consistent to previously published spectra of $LiFePO_4$. The main and the satellite binding energy positions of the Fe2p peaks perfectly match with the B.E. positions reported in literature and are characteristic for Fe^{2+} cations. Normally the B.E. separation between the Fe2p main peak and satellite peak indicates the Fe^{2+} and Fe^{3+} contribution in the sample. In comparison to spectra obtained for oxides the feature of the $2p_{3/2}$ emission can be assigned to a dominant contribution of Fe in its normal 2^+ oxidation state [29–31]. For our samples the B.E. separation between the Fe2p main peak and the satellite peak for pure $LiFePO_4$ and $LiFePO_4$–CNF samples is nearly 6 eV, which confirms that only Fe^{2+} contributions are present in the sample. For Fe^{3+} contributions the energy separation between main and satellite peaks would be 8 eV [31]. We were not able to deconvolute the main emission line as reported in [30] further due to limited resolution of the spec-

Table 2
XPS binding energies of various atoms for pure $LiFePO_4$ and $LiFePO_4$–CNF

Elements	Pure $LiFePO_4$ (eV)	$LiFePO_4$–CNF (eV)	Assignments
Oxygen	531.3	531.5	$LiFePO_4$
(O1s)		533.0	CNT (C—OH, C═O)
Carbon	284.2	284.2	CNT
(C1s)	286.1	285.6	CNT–OH
	288.2	289.3	CNT–CO
Phosphorus (P2p)	133.4	133.5	PO_4
Iron (Fe2p)			
	709.6	707.6	Defects
$Fe2p_{3/2}$	712.6	710.5	Fe^{2+}
	718.3	716.7	Satellite
$Fe2p_{1/2}$	726.0	724.1	Fe^{2+}
	732.7	730.2	Satellite

tra; despite the principle resolution power of our setup is below 0.4 eV. This is probably due to some inhomogeneity effects in slight charging and/or crystalline quality of our samples. A more detailed analysis of the photoemission feature will be performed in future experiments also considering the charges in oxidation states during charging (Li deintercalation).

3.2.6. Electrochemical measurements

Electrochemical measurements have been performed for pure $LiFePO_4$ and $LiFePO_4$–CNF samples. The elemental analysis for pure $LiFePO_4$ indicates the presence of 2.3 wt.% of carbon content in the sample and has been included in the calculation of the active mass. 12.3 wt.% of carbon content for the $LiFePO_4$–CNF sample has two origins, 10 wt.% from the functionalized CNFs (known amount) and around 2.3 wt.% from amorphous carbon, as calculated from elemental analysis. Hence 12.3 wt.% carbon has been included for active mass calculation for the $LiFePO_4$–CNF cathode sample. Fig. 11a and b shows the potential versus composition curves of $LiFePO_4$ and $LiFePO_4$–CNF electrode at 0.5C rate respectively. Fig. 12 represents the cycling performance of pure $LiFePO_4$ and $LiFePO_4$–CNF samples. The results indicate that the highly

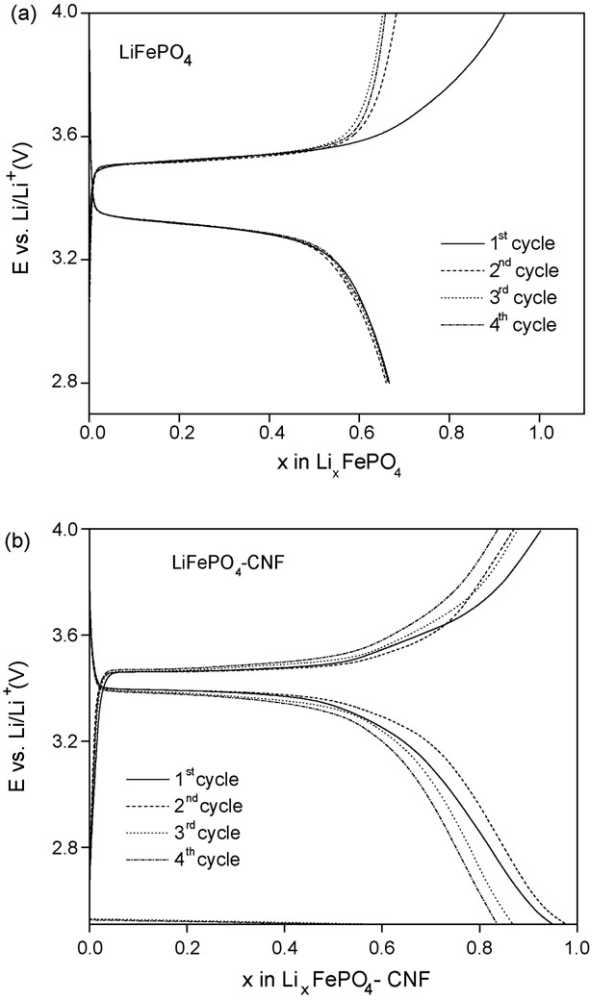

Fig. 11. Potential–composition curves of (a) $LiFePO_4$ at 0.5C and (b) $LiFePO_4$–CNF at 0.5C.

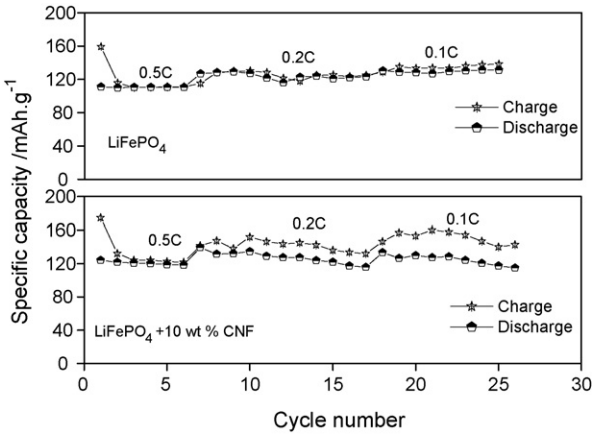

Fig. 12. Cycling performance of pure $LiFePO_4$ and $LiFePO_4$–CNF.

ordered pyrolytically stripped Carbon Nano Fibers improve the electrochemical performance of $LiFePO_4$–CNF cathodes with low carbon content (∼10 wt.%) in comparison with amorphous carbon black (∼25 wt.%) added to pure $LiFePO_4$. The specific structure of the carbon additives plays a dominant role for the resulting electrochemical performance [14]. Currently interface studies on the electrochemical behavior of $LiFePO_4$–CNF by in situ XPS and investigations of the rate capability are in progress.

4. Conclusion

$LiFePO_4$ particles coated over CNF fibers have been synthesized by a sol–gel method. An oxidative wet functionalization of Carbon Nano Fibers by concentrated HNO_3 gives better adhesion of $LiFePO_4$ particles on the CNF surfaces. The functionalized Carbon Nano Fiber added $LiFePO_4$ shows better electrochemical performance compared to acetylene black added $LiFePO_4$ even though the coating is not homogeneous. The results indicate that the specific structure of the composite electrode induced by the CNT plays a significant role in enhancing the electrochemical performance of $LiFePO_4$–CNF with simultaneously reduced carbon content, which is important for their practical use. The improved performance is probably due to the high electronic conductivity of the cathode material due to the CNF addition and the efficient contact between electrochemical active particles and the electronic conducting CNFs. The nanosized composite shortens the diffusion paths for lithium ions, increases the diffusion rate and results in better kinetic conditions in the electrode material. A more uniform coating of $LiFePO_4$ over the CNF layers is the next step to approach the theoretical capacity over large cycle numbers at high charging rates and with low carbon content.

Acknowledgement

Financial support from the *Deutsche Forschungsgemeinschaft* under grant nos. DFG JA859/14 and EH183/3 within the Priority Programme SPP 1181 "Nanoscaled Inorganic Materials by Molecular Design: New Materials for Advanced Technologies" is gratefully acknowledged.

References

[1] S.H. Wu, M.T. Yu, J. Power Sources 165 (2007) 660.
[2] J. Yao, S. Bealay, K. Konstantionov, V.A. Drozd, R.S. Liu, X.L. Wang, H.K. Liu, G.X. Wang, J. Alloys Compd. 425 (2006) 362.
[3] J. Wolfenstine, J. Allen, J. Power Sources 136 (2004) 153.
[4] Y. Wang, J. Wang, J. Yang, Y. Nuli, Adv. Funct. Mater. 16 (2006) 2135.
[5] A.K. Padhi, K.S. Nanjundaswamy, J.B. Goodenough, J. Electrochem. Soc. 144 (1997) 1188.
[6] M. Gaeberscek, R. Dominko, M. Bele, M. Remskar, D. Hanzel, J. Jamnik, Solid State Ionics 176 (2005) 1801.
[7] C. Delacourt, P. Poizot, S. Levasseur, C. Masquelier, Electrochem. Solid State Lett. 9 (7) (2006) A352.
[8] S.L. Bewlay, K. Konstantinov, G.X. Wang, S.X. Dou, H.K. Liu, Mater. Lett. 58 (2004) 1788.
[9] C.H. Mi, G.S. Cao, X.B. Zhao, Mater. Lett. 59 (2005) 127.
[10] Z.H. Chen, J.R. Dahn, J. Electrochem. Soc. 149 (2002) A1184.
[11] C.R. Sides, F. Croce, V.Y. Young, C.R. Martin, B. Scrosati, Electrochem. Solid-State Lett. 8 (2005) A484.
[12] J.F. Ni, H.H. Zhou, J.T. Chen, X.X. Zhang, Mater. Lett. 59 (2005) 2361.
[13] J. Yang, J.J. Xu, J. Electrochem. Soc. 153 (4) (2006) A716.
[14] Y. Hu, M.M. Doeff, R. Kostecki, R. Finones, J. Electrochem. Soc. 151 (8) (2004) A1279.
[15] P. Subramanya Herle, B. Ellis, N. Coombs, L.F. Nazar, Nat. Mater. 3 (2004) 147.
[16] K. Zaghib, J. Shim, A. Guerfi, P. Charest, K.A. Striebel, Electrochem. Solid. State Lett. 8 (4) (2005) A204.
[17] C.M. Julin, K. Zaghib, A. Mauger, M. Massot, A.A. Salah, M. Selmane, F. Gendron, J. Appl. Phys. 100 (2006) 063511.
[18] W.V. Zhihong, C.U. Pittman, S.D. Gardner, Carbon 33 (1995) 597.
[19] Y. Liu, C. Pan, J. Wang, J. Mater. Sci. 39 (2004) 1091.
[20] O.M. Teyssier, S.S. Valdes, L.F.R. Valle, Macromol. Mater. Eng. 291 (2006) 1547.
[21] S.F. Waseem, S.D. Gardner, G. He, W. Jiang, U. Pittmann, J. Mater. Sci. 33 (1998) 3151.
[22] S.D. Gardner, C.S.K. Singamsetty, Z. Wu, C.U. Pittmann, Surf. Interface Anal. 24 (1996) 311.
[23] R.W. Grimes, A.N. Fitch, J. Mater. Chem. 1 (3) (1991) 461.
[24] C.H. Lu, S.J. Liou, Ceram. Int. 25 (1999) 431.
[25] A. Yu, N. Kumagai, Z. Liu, J.Y. Lee, J. Power Sources 74 (1998) 117.
[26] V.A. Streltsov, E.L. Belokoneva, V.G. Tsirelson, N. Hansen, Acta Crystallogr. B49 (1993) 147.
[27] A. Caballero, M.C. Yusta, J. Morales, J.S. Pena, E.R. Castellón, Eur. J. Inorg. Chem. (2006) 1758.
[28] A.P. Grosvenor, B.A. Kobe, M.C. Biesinger, N.S. Mclntyre, Surf. Interface Anal. 36 (2004) 564.
[29] J. Lu, Z. Tang, Z. Zhang, W. Shen, J. Electrochem. Soc. 152 (7) (2005) A1441.
[30] P. Gratt, M.A.J. Somers, Surf. Interface Anal. 26 (11) (1998) 773.
[31] M. Aronniemi, J. Sainio, J. Lahtinen, Surf. Sci. 578 (2005) 108.